Hermes regulates axon sorting in the optic tract by post-transcriptional regulation of Neuropilin 1

Abbreviated title: Hermes regulates retinotectal projections.

Authors: Hanna Hörnberg *[1], Jean-Michel Cioni*, William A. Harris and Christine E. Holt[§]

Department of Physiology, Development and Neuroscience,
University of Cambridge, Downing Street, Cambridge, CB2 3DY
United Kingdom
[1]Current address: Biozentrum, University of Basel, Klingelbergstrasse 50/70, 4056 Basel, Switzerland

*These authors contributed equally to this work.

[§] Corresponding author

Email addresses:
CEH: ceh33@cam.ac.uk
WAH: wah20@cam.ac.uk
HH: hanna.hoernberg@unibas.ch
JMC: jmc235@cam.ac.uk

Number of pages: 15

Number of figures: 4

Number of words for Abstract: 168

Number of words for Introduction: 436

Number of words for Discussion: 1112

Acknowledgements: This work was supported by Wellcome Trust Programme Grants (085314) (CEH), European Research Council Advanced Grant (322817) (CEH), a Wellcome Trust Investigator Award (WAH), EMBO Long Term Fellowship (JMC), BBSRC studentship (HH) and Cambridge Gates Trust Scholarship (HH).

Conflict of interest: The authors declare no competing financial interests.

Abstract

The establishment of precise topographic maps during neural development is facilitated by the pre-sorting of axons in the pathway before they reach their targets. In the vertebrate visual system such topography is clearly seen in the optic tract and in the optic radiations. However, the molecular mechanisms involved in pre-target axon sorting are poorly understood. Here we show that in zebrafish the RNA-binding protein, Hermes, which is expressed exclusively in retinal ganglion cells (RGCs), is involved in this process. Using a RiboTag approach, we show that Hermes acts as a negative translational regulator of specific mRNAs in RGCs. One of these targets is the guidance cue receptor Neuropilin 1 (Nrp1) which is sensitive to the repellent cue Semaphorin 3A (Sema3A). Hermes knockdown leads to topographic missorting in the optic tract through the up-regulation of Nrp1. Restoring Nrp1 to appropriate levels in Hermes-depleted embryos rescues this effect and corrects the axon sorting defect in the optic tract. Our data indicate that axon sorting relies on Hermes-regulated translation of Nrp1.

Significance statement

An important mechanism governing the formation of the mature neural map is pre-target axon sorting within the sensory tract, however the molecular mechanisms involved in this process remain largely unknown. The work presented here reveals a novel function for the RNA-binding protein Hermes, in regulating the topographic sorting of retinal ganglion cell (RGC) axons in the optic tract and tectum. We find that Hermes negatively controls the translation of the guidance-cue receptor Neuropilin-1 in RGCs, with Hermes knockdown resulting in aberrant growth cone cue-sensitivity and axonal topographic misprojections. We characterize a novel RNA-based mechanism by which axons developmentally restrict their translatome in order to achieve proper targeting.

Introduction

In the vertebrate visual system, retinal ganglion cells (RGCs) project topographically to the optic tectum (superior colliculus in mammals) along the anterior–posterior (A-P) and dorsal–ventral (D-V) axis. This topography is established, as first postulated by Roger Sperry (Sperry, 1963), by the graded expression of guidance cues (e.g. Ephrins) at the target which guide RGC axons that express graded amounts of the receptors (Ephs) for these cues (Feldheim and O'Leary, 2010). Interestingly, however, RGC axons are already topographically sorted in the optic tract (OT) before reaching their target (Scholes, 1979; Fawcett et al., 1984; Stuermer, 1988; Plas et al.,

2005). This sorting occurs only after the axons have crossed the optic chiasm, indicating it is precisely regulated. Differential expression of Neuropilin 1 (Nrp1) and Semaphorin3A (Sema3A) have been shown to regulate the correct pre-target topographic position of axons in the olfactory system and corpus callosum (Imai et al., 2009; Zhou et al., 2013).

Post-transcriptional regulation has emerged as a key mechanism to temporally regulate protein expression in axons during development (Holt and Schuman, 2013; Batista and Hengst, 2016; Jain and Welshhans, 2016). RNA-binding proteins (RBPs) play a crucial part in this process (Hornberg and Holt, 2013), and several RBPs have been implicated in axon guidance and target recognition (McWhorter et al., 2003; Yao et al., 2006; Li et al., 2009; Glinka et al., 2010; Ymlahi-Ouazzani et al., 2010; Welshhans and Bassell, 2011). Of particular relevance to this study is work by Chien and colleagues showing that the fragile-X interacting protein CYFIP2 (cytoplasmic FMR1 interacting protein 2), a protein linked to RNA-regulation, causes tract-sorting errors of dorsal axons in the optic tract (Pittman et al., 2010). This result indicates that translational regulation may be involved in the sorting of RGC axons. We have previously shown that the RBP, Hermes (RBPMS, RNA-binding protein with multiple splicing), is exclusively expressed in RGCs during and after axogenesis but its mechanism of action is unknown (Hörnberg et al., 2013).

Here, we investigate the role of Hermes during axon sorting in the optic tract of zebrafish and *Xenopus laevis*. We find that Hermes knock-down induces topographic errors in the positioning of dorsal axons in the optic tract, which leads many to enter the tectum medially rather than laterally. We identify several mRNAs whose expression is specifically down-regulated by Hermes in RGCs, including the Semaphorin3A-sensitive guidance receptor Neuropilin1 (Nrp1). Reducing excessive Nrp1 activity in Hermes-depleted zebrafish embryos is sufficient to restore correct topographic sorting of dorsal axons the optic tract. Taken together, these findings demonstrate a critical role for Hermes as a translational regulator during topographic map formation in the visual system.

Materials and Methods

Embryo maintenance

Xenopus embryos were obtained by *in vitro* fertilization, raised in 0.1X Modified Barth's Saline at 14°C-20°C and staged according to the tables of Nieuwkoop and Faber (1967). Zebrafish embryos of either sex were obtained from WT (AB-TL or TL) strains, maintained and bred at 26.5°C. The stable transgenic atoh7:rpl10a-GFP line was obtained by using Tol2 system (Suster et al., 2009). Embryos were raised at 28.5°C in E3 embryo medium. Embryos to be collected for

fluorescent imaging had the embryo medium supplemented with 0.003% phenylthiourea (PTU, Sigma) for pigment reduction. All animal work was approved by Local Ethical Review Committee at the University of Cambridge and performed according to the protocols of project license PPL 80/2198.

DNA constructs and morpholinos

All constructs were expressed in the pCS2+ vector (David Turner, University of Michigan, Ann Arbor). Xenopus hermes cDNA (Genbank GeneID AF107889) was kindly provided by Dr. M. Kloc and sublconed in pCS2+ with an N-terminally myc tag. The stable line was made by cloning *atoh7* promoter (Zolessi et al., 2006) into Tol2 zTRAP vector (addgene, 42236). Morpholinos (MOs) were obtained from Gene Tools. Xenopus hermes and control MOs were conjugated to FITC and were designed exactly as described previously by Zearfoss et al., (2004). Xenopus hermes a-MO: GCCCACCGAGGAGTCTGGCTTGTAC and Xenopus hermes b-MO: ATGAGCGGCATCAAGTCAGACACGG were injected at 2.5 ng each. The following zebrafish MOs and concentrations were used:

hermes1a (rbpms2b) – CTTGACACTCATCTTGTGCGTAAAC, 8 ng

hermes1b (rbpms2a) – TTCAGACTCATTGTGTAACTTTAAC, 8 ng

Both MOs have been verified previously (Hörnberg et al., 2013).

nrp1a – GAATCCTGGAGTTCGGAGTGCGGAA, 190 pg

Zebrafish embryo injection

MOs were injected into the yolk of zebrafish embryos at the 1-2 cell stage. Embryos were lined up on a plastic dish against a glass slide in a medium free environment. Injections were performed using 0.78mm needles pulled with a needle puller (1.0 mm OD x 0.78 mm, Harvard Aparatus; puller: Pul-1, World Precision Instrument) and 0.5-2 nl of volume was pressure injected using an air-pressure injector (Picospritzer II, Intracel).

Translating Ribosome Affinity Purification (TRAP)

Heads were dissected from 72hpf atoh7:rpl10a-GFP and atoh7:gap-GFP embryos (n=75 /condition) in E3 embryo medium containing cycloheximide (SIGMA, 100 µg/ml) and MS222, snap-frozen on dry ice and stored at -80°C. Tissues were homogenized in lysis buffer (20mM Tris-HCL (pH 7.4), 5mM $MgCl_2$, 150mM KCl, 1% NP40, RNAse OUT (1U/µl) and Complete EDTA-free Protease Inhibitor Cocktail) supplemented with cycloheximide (100 µg/ml), incubated at 4°C for 30min and centrifuged at 4°C, 20,000g, for 20min. The supernatant was then collected and 10% of the extract has been kept for total RNA extraction. The rest of the extract was then used for ribosome-mRNA complex immunoprecipitation with an anti-GFP antibody (Abcam Cat# ab6556, RRID:AB_305564) pre-conjugated to Protein G-magnetic beads (Dynabeads Protein G, Life Technologies 10004D). After 4 washes with lysis buffer, the total RNA was extracted from the ribosome-mRNA complex using an RNeasy mini kit (Qiagen), followed by in-column DNase treatment to remove genomic DNA contamination. The RNA quality and quantity was then

measured on the Agilent 2100 Bioanalyser System (Agilent technologies) and the atoh7:gap-GFP condition allowed us to verify the immunoprecipitation specificity. cDNA synthesis was then performed using the superscript III first-strand synthesis system (Invitrogen) and quantified by lightcycler 480 (Roche).

Xenopus embryo injection

Embryos were injected as previously described (Vignali et al., 2000). Injections were performed at the 4- or 8-cell stage in both dorsal-animal blastomeres. Embryos were de-jellied with 2% cysteine (Sigma) in 1xMBS (pH 8), rinsed 3x in 0.1xMBS and lined up on a grid in 4% Ficol (Sigma) in 0.1xMBS, 1% penicillin (100 U/ml), streptomycin (100 mg/ml) and fungizone 0.25 mg/ml (PSF, GIBCO). 5 ng (2.5 each) of HeMOs were injected using glass capillary needles (1.0 mm OD x 0.5 mm, Harvard Aparatus) and a microinjector (Picospritzer, General Valve).

Xenopus Retinal explant cultures

50 mm glass-bottom dishes (Matek) were coated overnight at 20°C or at room temperature (RT) for a minimum of 3 h with poly-L-lysine (PLL; 10 µg/ml) in double distilled H2O (ddH2O), followed by coating with laminin (10 µg/ml, Sigma) in L-15 medium (Gibco) for 1 h at RT. Embryos jelly coat were removed using forceps. All embryos were washed 3x in 0.1X MBS with 1% PSF to remove bacteria. Embryos were placed on a Sylgard coated dish in a 1:1 mixture of 60% L-15 culture medium (60% L-15 in ddH2O and 1% PSF, pH 7.6-7.8) and MS222. Anesthetized embryos were pinned down with custom made pins and the eye dissected out using dissection pins. Whole eye or eye pieces were then washed in 60% L-15 and plated on precoated dishes containing 60% L-15 culture medium with the lens side up. Dishes were incubated at 20°C for 12-24 h depending on the experiment.

Collapse assays

Stage 28-40 retinal explants were cultured for 24 h at 20°C. For Semaphorin3A collapse assay, cultures were treated with either 450 ng/mL recombinant human Semaphorin3A Fc chimera (R&D Systems) in 0.1% protease free bovine serum albumin (BSA, Sigma) or 0.1% BSA for 10 min followed by fixation in 4% paraformaldehyde (PFA) containing 15% sucrose (Sigma) in 1x PBS. All growth cone collapse was counted blind. Collapse was quantified as growth cones lacking lamellipodia and having two or fewer filopodia.

Lipophilic dye labelling and imaging

Topographic analysis was done at 5dpf when the tectum is first fully innervated. Morpholino injected zebrafish embryos were fixed with 4% PFA at 5 dpf and kept at 4^{o}C for a minimum of 24 h. Embryos were pinned down on a custom-made Sylgard plate in 1x PBS. The different quadrants in the retina were pressure-injected using a microinjector (Picospritzer, General Valve) and 0.5 mm needles pulled as previously described. Ventral and temporal retina was injected with 3,3'-dioctadecyloxacarbocyanine perchlorate (DiO, Molecular Probes) dissolved in dimethylformamide (DMF, Sigma), and dorsal and nasal retina with 1,1'-dioctadecyl-3,3,3',3'-

tetramethylindocarbocyanine perchlorate (DiI, Molecular Probes) dissolved in 100% ethanol (Sigma). After 12-24 h incubation in the dark at RT, embryos were examined under epifluorescence and only embryos with perfect targeting in the eye were used for further analysis. For visualization of labelled axons, both eyes were removed using dissection pins and embryos were mounted either dorsally or laterally in a custom-made glass bottom dish in 1.2% low melting point agaros (24–28°C gelling point, Promega). Images were acquired using a Perkin Elmer Spinning Disk UltraVIEW ERS, Olympus IX81 Inverted microscope and 20x (0.45 NA) or 60x (1.2 NA) water immersion objective. Images were acquired using Volocity 3D Image Analysis Software (RRID:SCR_002668, Perkin Elmer). All analysis was performed blind to the morpholino knockdown.

Puromycin assay

Zebrafish embryos (48hpf) were incubated in in E3 embryo medium containing 200µg/ml of puromycin (Sigma). Fish heads were dissected at 72 hpf and homogenized in RIPA buffer (Sigma) supplemented with Halt protease and phosphatase inhibitor cocktail (Invitrogen). Proteins were resolved by 10% SDS-PAGE and transferred to nitrocellulose membrane (BioRad). Antibodies used were mouse anti-puromycin (1:1000, Millipore Cat# MABE343, RRID:AB_2566826) and mouse anti-alpha-tubulin (1:10000; Sigma-Aldrich Cat# T6074, RRID:AB_477582) antibodies, followed by horseradish peroxidase-conjugated secondary antibody (Abcam Cat# ab6789, RRID:AB_955439). Bands were detected using an ECL-based detection (GE Healthcare).

Immunohistochemistry

Eye explant cultures from Xenopus were fixed in 4% PFA and 15% sucrose in 1x PBS for 30 min, washed 3x10 min in 1x PBS and permeabilized for 5 min in 0.1% triton (Sigma) in 1x PBS. The explants were gently washed 3 more times in 1x PBS and blocked for 30 min in 5% heat inactivated goat serum (HIGS). Primary antibodies were diluted in 5% HIGS and added to the explants for 1 h at RT. The explants were then washed 3x10 in PBS before incubation with the secondary antibody in 1x PBS for 45 min at RT. The explants were washed a final 3 times in 1x PBS before mounted with FluorSave reagent (Calbiochem) or imaged directly in 1x PBS.
For immunostaining on cryostat sections, zebrafish embryos were fixed for 1-2 h in 4% PFA at RT, rinsed 3x in 1x PBS and put in 30% sucrose in 1x PBS for a minimum of 30 min. Embryos were embedded in Tissue-TEK OCT compound (SAKURA) and quick frozen on dry ice or at -80°C. Transverse retina or brain sections with a 10 µm thickness were cut using a cryostat (Leica CM3050S). Slides were washed 3x 10 min in PBS and permeabilized in 0.2% Tween (Sigma) in 1x PBS before blocked for 1 h in blocking buffer (0.1% BSA, 10% HIGS, 0.1% Triton, 1x PBS). Primary antibodies were incubated over night (O/N) at RT in a humidified chamber. Slides were then washed 3x in 1x PBS and incubated with secondary antibody for 1 h at RT in a humidified chamber in the dark. Slides were washed a final 3x 10 min in PBS, incubated with

1:10000 DAPI for 45 min in a humidified chamber at RT, drained of and mounted with FluorSave reagent. All slides were imaged using a Perkin Elmer Spinning Disk UltraVIEW ERS, Olympus IX81 Inverted microscope and 20x (0.45 NA) objective. The following primary antibodies were used: anti-myc-tag (Abcam Cat# ab32, RRID:AB_303599) 1:5000, anti-Zn5 (Zebrafish International Resource Center Cat# zn-5, RRID:AB_10013770) 1:500 and anti-Nrp1 (gift from H. Fujisawa) 1:50.

Results

Hermes depletion disrupts topography of dorsal axons in optic tract and tectum

Hermes knockdown can be efficiently achieved in zebrafish by injecting antisense morpholinos (MOs) targeted to both *hermes1a* and *hermes1b* zebrafish transcripts (Hörnberg et al., 2013). We have previously showed that Hermes knockdown interferes with RGC synapse formation and arborization in the optic tectum (Hörnberg et al., 2013). To study the effect on topography, we used the lipophilic dyes DiI and DiO to label the dorsal and ventral part of the retina separately (Fig.1 A). Dye injections were performed at 5 days post-fertilization (dpf), when the tectum is first fully innervated. At this stage, dorsal and ventral axons are clearly segregated along the optic tract, with dorsal axons projecting through the lateral branch and ventral axons through the medial branch (Stuermer, 1988; Poulain and Chien, 2013). In control morpholino injected embryos (CoMO), we see the same result (Fig.1 B1-B2). In Hermes-depleted embryos (HeMO), however, dorsal axons were frequently observed ectopically in the medial branch of the optic tract (Fig.1 C1-C2), leading to a significant increase in the percentage of embryos with tract sorting defects compared to control embryos ($p<0.001$, Fisher's exact test, Fig.1 D). Interestingly, ventral axons appeared to navigate correctly along the optic tract in HeMO injected embryos, indicating that only dorsal axons were affected by Hermes depletion (Fig.1 C1-C2). In control embryos, dorsal axons reached the tectum through the lateral branch and projected directly to their target area in the medial tectum (Fig.1 B3). In HeMO injected embryos, however, dorsal axons frequently entered the tectum aberrantly through the medial branch and then followed a circuitous route to the medial tectum (Fig.1 C3). In CoMO larvae, few if any axons made guidance errors on entering the tectum while in HeMO embryos there were many (control: 0.91 ± 0.50, HeMO: 7.20 ± 1.27, $p< 0.0001$, Mann Whitney test, Fig.1 E).

In morpholino-based studies, it is critical to test the specificity of the induced phenotype. We therefore performed a rescue experiment by injecting a construct expressing a myc-tagged *Xenopus laevis* Hermes sequence (He-myc) into HeMO injected zebrafish embryos (Fig.1 F). *Xenopus* Hermes mRNA has a high sequence similarity to zebrafish but is not targeted by the zebrafish HeMOs. We first confirmed the construct expression by coronal sections of HeMO and

He-myc co-injected embryos showing strong Myc expression in the RGC layer (RGCL) (Fig.1 F). We next examined the retinotectal topography of Hermes morphants at 5 dpf, with or without co-injection of He-myc. Co-injection of He-myc in HeMO injected embryos significantly reduced the amount of embryos with misprojected dorsal axons compared to embryos injected with HeMO only, resulting in a percentage similar to control ($p<0.05$, Fisher's exact test, Fig.1 G, H). Likewise, expression of He-myc was found to reduce the D-V sorting defect in the optic tectum observed after Hermes knockdown ($p<0.05$, One-way ANOVA, Fig.1 I-L). Thus, the injection of *Xenopus* Hermes rescues the misrouting of dorsal axons observed in HeMO injected zebrafish embryos, indicating that the phenotype observed in these embryos is specific to Hermes depletion.

Hermes negatively regulates the translation of specific mRNAs in RGCs

To investigate whether Hermes acts to repress or enhance translation in the zebrafish nervous system, we decided to quantify the global protein synthesis by using puromycin incorporation into nascent peptide chains (Lin et al., 2009). Western blot analysis of 72 hpf embryo brain and eye extracts showed a significant increase of puromycin immunoreactivity in HeMO injected embryos compared to control (Mann Whitney test, Fig. 2 A, B). This increase, indicative of a rise in protein synthesis, suggests that Hermes normally acts as a translational repressor.

We next sought to determine which mRNAs were specifically repressed in RGCs after Hermes depletion using a riboTRAP approach. We generated a zebrafish transgenic line in which the ribosomal protein rpl10a was tagged with GFP and its expression was under the control of the atoh7 promoter (atoh7:rpl10a-GFP) (Tryon et al., 2013) (Fig.2 C). As expected, rpl10a-GFP expression was limited to the eye (Fig.2 C1-C2), with positive signal detected in the RGC (visualized with Zn-5 staining, Fig.2 C2-C4) and photoreceptor layers (Fig.2 C1-C4). In order to isolate ribosome-associated mRNAs from RGC cell bodies and axons, rpl10a-GFP immunoprecipitation was performed on eyes and brains from HeMO or CoMO injected embryos collected at 72 hpf (Fig.2 D). We then performed a quantitative RT-PCR analysis on 11 genes known to be involved in sensory topography map formation (Fig.2 E). Six housekeeping genes were selected for normalization. Out of the 11 genes analyzed, 6 showed a significantly higher amount of ribosome-bound mRNA after Hermes knockdown compared to control, with no change observed for the others (n=3 experiments, Mann Whitney test, Fig.2 E). The 6 genes that showed increased translation in the HeMO condition were found to correspond to the zebrafish duplicated genes of the mammalian orthologues of the cell adhesion molecules L1cam (*nadl1.1*, *nadl1.2*) and ALCAM (*alcama*, *alcamb*), and the guidance receptor Neuropilin1 (*nrp1a*, *nrp1b*) (Fig.2 E).

It is possible that the increased ribosome-association of these 6 mRNAs is due to an overall increase on their abundance. To examine this, we first did a quantitative RT-PCR analysis for the 6 mRNAs from total RNA extracts (Fig.2 F). These results showed no significant difference in the amounts of message between CoMO and HeMO conditions for the 6 mRNAs analyzed (n=3 experiments, Mann Whitney test) indicative of no difference in overall mRNA abundance. We also performed *in situ* hybridisations for *nrp1* mRNA on transverse sections of 72hpf HeMO and CoMO injected embryos (Fig.2 G). Again, we observed no obvious change in the localization, and quantification of signal intensity (n.s, Mann Whitney test, Fig.2 G). Taken together, these results showed a specific function for Hermes in RGCs as a negative translation regulator of restricted target mRNAs.

Hermes depletion increases Nrp1 in RGC growth cones and confers premature sensitivity to Sema3A

Previous *Xenopus laevis* studies, have shown precise, intrinsic regulation of Nrp1 expression in RGCs during development, with a sharp stage-dependent increase of the protein in axons and growth cones (Campbell et al., 2001). Delaying the expression of Nrp1 by MO injection was found to induce pathfinding errors in the optic tract by interfering with the growth cone's responsiveness to Semaphorin 3A (Sema3A) (Baudet et al., 2012). We hypothesized that Hermes functions to restrict Nrp1 levels in RGC growth cones, thereby regulating their sensitivity. Using Xenopus retinal explants, we examined Nrp1 expression levels in RGC axons and growth cones (Fig.3 A-E). Quantification of Nrp1 immunoreactivity showed a significant increase in Hermes-depleted RGC growth cones compared to control growth cones (Fig.3 A). This increase was found throughout RGC axon development (Fig.3 B-E).

To test whether higher levels of Nrp1 in growth cones would be sufficient to induce a precocious cue response, we tested the sensitivity to Sema3A by performing a collapse assay (Fig.3 F-I). As previously observed, retinal explants from stage 32 cultured for 24h were not sensitive to Sema3A (Fig.3 H; (Campbell et al., 2001; Baudet et al., 2012), whereas a significant Sema3A-induced collapse was seen in explants from stage 35/36 embryos (Fig.3 I). In contrast, explants from stage 32 HeMO-morphant eyes displayed a significant Sema3A-induced collapse response (Fig. 3 H), which was also present at stage 35/36 (Fig.3 I). These results show that the regulation of intrinsic Nrp1 levels is Hermes-dependent in RGCs and controls growth cone cue-sensitivity.

Nrp1 rescues the guidance errors of dorsal axons in Hermes-depleted RGCs

The above findings suggest that the missorting of dorsal axons in the optic tract of Hermes-depleted embryos may be caused by dysregulated translation of Nrp1 leading to premature and

aberrant expression of Nrp1 in retinal growth cones. To examine this idea, we first asked if Nrp1 expression was increased *in vivo* in Hermes-depleted eyes. As expected, immunostaining on 72hpf zebrafish retina showed a significant increase in Nrp1 expression in Hermes-depleted embryos compared to control (Kruskal-Wallis test, Dunn's multiple comparison Fig.4 A-D).
We next tested whether the guidance errors observed in Hermes morphants were caused by the elevated levels of Nrp1 by reducing the expression of Nrp1 in HeMO embryos. To do this, we used a low dose of Nrp1MO (190pg) (Fig.4 C, D). As previously shown, Hermes depletion alone caused a significant increase in the percentage of embryos with missorted dorsal axons compared to control embryos at 5 dpf ($p<0.01$, Chi-square test, Fig.4 E-H). However, co-injection of 190pg of Nrp1MO reduces the percentage of embryos with guidance errors in the optic tract to 28%, significantly lower than HeMO injected embryos and similar to the percentage of missorting found in control-injected embryos ($p<0.01$, Chi-square test, Fig.4 G, H). The rescue of tract missorting is reflected in the targeting of dorsal axons in the tectum, which showed a significant decrease in Nrp1MO co-injected embryos compared to embryos injected with HeMO alone ($p<0.05$, Kruskal-Wallis test, Dunn's multiple comparison test, Fig.4 I-L). These results demonstrate that the topographic errors of dorsal axons in Hermes-depleted embryos are at least partially due to dysregulated Nrp1 expression.

Discussion

In this study, we show that the RBP Hermes regulates the sorting of RGC axons in the optic tract. Our data revealed that Hermes functions as a translational repressor by negatively regulating the translation of specific mRNAs in RGCs. We show that Hermes is important for the intrinsic control of Nrp1 expression in the growth cone and thus its sensitivity to extracellular cues such as Sema3A. Furthermore, we found that reducing the level of Nrp1 in Hermes-depleted embryos was sufficient to rescue the guidance errors of dorsal axons. Thus, this study demonstrates a novel role for RBP-mediated post-transcriptional control in topographic map formation by regulating the precise stage-dependent changes in growth cone responsiveness. Our results indicate that Hermes is a repressor of *nrp1* mRNA translation, either directly or indirectly, which temporally controls Nrp1 expression in RGC growth cones. Interestingly, the mammalian orthologue of Hermes, RBPMS2, has also been shown to bind to *nrp1*mRNA (Farazi et al., 2014).

How does misregulation of Nrp1 expression lead to topographic presorting defects? As is the case for the bulb-olfactory system, it is possible that Nrp1 expression enables RGC dorsal axons to respond to a repulsive cue topographically expressed by either an intermediate target along the path or by the ventral RGC axons (Imai et al., 2009). Several Semaphorins are expressed in

the RGC layer or along the optic tract (Kuwajima et al., 2012). Surprisingly, knockdown of class III Semaphorins does not seem to affect the topographic projections of RGC axons *in vivo* (data not shown). However, the vascular endothelial growth factor 164 (VEGF-164), another Nrp1 ligand, displays an expression along the RGC axonal pathway and mice lacking VEGF-164 show defasciculation of the optic tract, indicating a potential role in tract sorting (Erskine et al., 2011). A second possibility is that Nrp1 regulates homotypic fasciculation between RGC axons. Indeed, Nrp1 has been shown to regulate axon-axon interactions in motor neurons (Huettl et al., 2011). Thus, Nrp1 expression in RGC growth cones may play a role during homotypic and/or heterotypic axon-axon cell-contact recognition. A third possibility relates to the fact that the path of dorsal RGC axons is refined during development (Poulain and Chien, 2013). This would result from degeneration of mistargeted RGC axons in zebrafish between 50 and 72hpf (Poulain and Chien, 2013). Consistent with this suggestion is the finding that Nrp1 is required for axonal pruning during development (Bagri et al., 2003). Further studies are needed to distinguish between these hypotheses and define the molecular mechanisms through which Nrp1 expression affects axon sorting in the optic tract.

We have previously shown that Hermes depletion reduces RGC arbor complexity in zebrafish using single axon tracing and analysis (Hörnberg et al., 2013). The topographic origin of the axons was not known in this previous study so the axon sorting errors described here were not detected. It is possible that missorted dorsal axons have a more severe arborization phenotype. The elevated Nrp1 levels at 3dpf coincides temporally with the first observed alterations in branch dynamics in Hermes morphants (Hörnberg et al., 2013), thus suggesting that the increased Nrp1 levels could play a role in the reduced arborization. Indeed, Sema3A was found to increase RGC branch formation *in vitro* (Campbell et al., 2001), and Nrp1-Sema3A signaling regulates layer-specific branching in the mouse cerebellum (Cioni et al., 2013). However, in zebrafish, branching contributes to pathfinding via selective stabilization of branches formed toward the topographically correct target zone (Simpson et al., 2013). In Hermes depleted embryos, branch stability is unaffected, thus suggesting that Hermes may regulate topographic sorting and arborization via different mechanisms.

We have shown that Hermes expression in RGCs is critical to restrain the levels of Nrp1 expression in the growth cone through the different developmental stages, and that the experimental knock-down of Hermes leads to the precocious upregulation of Nrp1, increased sensitivity to Sema3A, and tract sorting errors. There are several questions that our study has not been able to resolve. One of these is whether the tract sorting defect observed in the absence of Hermes results from precocious Nrp1 expression during early stages of tract formation or the continuously elevated levels of Nrp1 throughout axon elongation in the optic

tract. To answer this question it will be essential to gain precise temporal control of Nrp1 expression. Another question concerns other factors that control Nrp1 expression. For example, it is known that Nrp1 levels rise after stage 32 (32hpf) even though Hermes continues to be expressed in RGCs (Hörnberg et al., 2013). In this regard, it is interesting to note that the onset of Nrp1 expression in RGCs is indirectly regulated by the microRNA miR-124 targeting of RE1 silencing transcription factor co-repressor 1 (CoREST), a transcriptional co-repressor (Baudet et al., 2012). The expression of miR-124 is upregulated and CoREST downregulated over time, allowing the increase of Nrp1 expression. The function of the mammalian orthologue of Hermes, RBPMS2, in RGCs has not been characterized, however, transcriptome analyses after optic nerve injury reveal a down-regulation of RBPMS2 concomitant with an increase of Nrp1 levels in RGC axons (Yasuda et al., 2014; Han et al., 2015; Yasuda et al., 2016), and rescue of RGC degeneration can be achieved by decreasing Nrp1 function (Shirvan et al., 2002). The parallels between these findings and those described in this paper suggest that this protective effect on mammalian optic axons may be achieved by similar molecular mechanisms. Finally, our study does not address whether the translation regulation of Hermes occurs in the axon and/or the cell body. Previous work has not detected the presence of *nrp1* mRNA in RGC axons, nor its translation (Zivraj et al., 2010; Shigeoka et al., 2016), however, it may have escaped detection due to low mRNA abundance and tight translational regulation. Hermes protein is expressed in RGC axons and is detected in growth cones (Hörnberg et al., 2013), opening the possibility of a local function. It is worth noting that the two other Hermes mRNA targets identified in this study, Nadl1 and Alcam, have been identified in growth cones (Zivraj et al., 2010; Thelen et al., 2012). Both have been implicated in the mapping of ventral axons in the mouse visual system (Demyanenko and Maness, 2003; Buhusi et al., 2008; Buhusi et al., 2009), thus raising the possibility that Hermes may locally regulate additional aspects of pathfinding via its other mRNA targets.

In summary, we have shown that Hermes acts as a translational repressor of Nrp1 expression in RGCs and this regulation is important for correct axonal sorting in the optic tract. While important questions remain, the evidence we provide demonstrates a new RNA-based molecular mechanism that operates during axonal navigation to regulate specific guidance receptors and affect accurate pathfinding decisions.

References

Bagri A, Cheng HJ, Yaron A, Pleasure SJ, Tessier-Lavigne M (2003) Stereotyped pruning of long hippocampal axon branches triggered by retraction inducers of the semaphorin family. Cell 113:285-299.

Batista AF, Hengst U (2016) Intra-axonal protein synthesis in development and beyond. Int J Dev Neurosci.

Baudet ML, Zivraj KH, Abreu-Goodger C, Muldal A, Armisen J, Blenkiron C, Goldstein LD, Miska EA, Holt CE (2012) miR-124 acts through CoREST to control onset of Sema3A sensitivity in navigating retinal growth cones. Nat Neurosci 15:29-38.

Buhusi M, Schlatter MC, Demyanenko GP, Thresher R, Maness PF (2008) L1 interaction with ankyrin regulates mediolateral topography in the retinocollicular projection. The Journal of neuroscience : the official journal of the Society for Neuroscience 28:177-188.

Buhusi M, Demyanenko GP, Jannie KM, Dalal J, Darnell EP, Weiner JA, Maness PF (2009) ALCAM regulates mediolateral retinotopic mapping in the superior colliculus. The Journal of neuroscience : the official journal of the Society for Neuroscience 29:15630-15641.

Campbell DS, Regan AG, Lopez JS, Tannahill D, Harris WA, Holt CE (2001) Semaphorin 3A elicits stage-dependent collapse, turning, and branching in Xenopus retinal growth cones. J Neurosci 21:8538-8547.

Cioni JM, Telley L, Saywell V, Cadilhac C, Jourdan C, Huber AB, Huang JZ, Jahannault-Talignani C, Ango F (2013) SEMA3A signaling controls layer-specific interneuron branching in the cerebellum. Curr Biol 23:850-861.

Demyanenko GP, Maness PF (2003) The L1 cell adhesion molecule is essential for topographic mapping of retinal axons. The Journal of neuroscience : the official journal of the Society for Neuroscience 23:530-538.

Erskine L, Reijntjes S, Pratt T, Denti L, Schwarz Q, Vieira JM, Alakakone B, Shewan D, Ruhrberg C (2011) VEGF signaling through neuropilin 1 guides commissural axon crossing at the optic chiasm. Neuron 70:951-965.

Farazi TA, Leonhardt CS, Mukherjee N, Mihailovic A, Li S, Max KE, Meyer C, Yamaji M, Cekan P, Jacobs NC, Gerstberger S, Bognanni C, Larsson E, Ohler U, Tuschl T (2014) Identification of the RNA recognition element of the RBPMS family of RNA-binding proteins and their transcriptome-wide mRNA targets. RNA 20:1090-1102.

Fawcett JW, Taylor JS, Gaze RM, Grant P, Hirst E (1984) Fibre order in the normal Xenopus optic tract, near the chiasma. J Embryol Exp Morphol 83:1-14.

Feldheim DA, O'Leary DD (2010) Visual map development: bidirectional signaling, bifunctional guidance molecules, and competition. Cold Spring Harbor perspectives in biology 2:a001768.

Glinka M, Herrmann T, Funk N, Havlicek S, Rossoll W, Winkler C, Sendtner M (2010) The heterogeneous nuclear ribonucleoprotein-R is necessary for axonal beta-actin mRNA translocation in spinal motor neurons. Human molecular genetics 19:1951-1966.

Han F, Huo Y, Huang CJ, Chen CL, Ye J (2015) MicroRNA-30b promotes axon outgrowth of retinal ganglion cells by inhibiting Semaphorin3A expression. Brain Res 1611:65-73.

Holt CE, Schuman EM (2013) The central dogma decentralized: new perspectives on RNA function and local translation in neurons. Neuron 80:648-657.

Hornberg H, Holt C (2013) RNA-binding proteins and translational regulation in axons and growth cones. Front Neurosci 7:81.

Hörnberg H, Wollerton-van Horck F, Maurus D, Zwart M, Svoboda H, Harris W, Holt C (2013) RNA-Binding Protein Hermes/RBPMS Inversely Affects Synapse Density and Axon Arbor Formation in Retinal Ganglion Cells In Vivo. The Journal of neuroscience : the official journal of the Society for Neuroscience 33:10384-10395.

Huettl RE, Soellner H, Bianchi E, Novitch BG, Huber AB (2011) Npn-1 contributes to axon-axon interactions that differentially control sensory and motor innervation of the limb. PLoS biology 9:e1001020.

Imai T, Yamazaki T, Kobayakawa R, Kobayakawa K, Abe T, Suzuki M, Sakano H (2009) Pre-target axon sorting establishes the neural map topography. Science 325:585-590.

Jain S, Welshhans K (2016) Local translation of cell adhesion molecules in axons. Neural Regen Res 11:543-544.

Kuwajima T, Yoshida Y, Takegahara N, Petros TJ, Kumanogoh A, Jessell TM, Sakurai T, Mason C (2012) Optic chiasm presentation of Semaphorin6D in the context of Plexin-A1 and Nr-CAM promotes retinal axon midline crossing. Neuron 74:676-690.

Li C, Bassell GJ, Sasaki Y (2009) Fragile X Mental Retardation Protein is Involved in Protein Synthesis-Dependent Collapse of Growth Cones Induced by Semaphorin-3A. Frontiers in neural circuits 3:11.

Lin AC, Tan CL, Lin CL, Strochlic L, Huang YS, Richter JD, Holt CE (2009) Cytoplasmic polyadenylation and cytoplasmic polyadenylation element-dependent mRNA regulation are involved in Xenopus retinal axon development. Neural Dev 4:8.

McWhorter ML, Monani UR, Burghes AH, Beattie CE (2003) Knockdown of the survival motor neuron (Smn) protein in zebrafish causes defects in motor axon outgrowth and pathfinding. The Journal of cell biology 162:919-931.

Pittman AJ, Gaynes JA, Chien CB (2010) nev (cyfip2) is required for retinal lamination and axon guidance in the zebrafish retinotectal system. Developmental biology 344:784-794.

Plas DT, Lopez JE, Crair MC (2005) Pretarget sorting of retinocollicular axons in the mouse. The Journal of comparative neurology 491:305-319.

Poulain FE, Chien CB (2013) Proteoglycan-mediated axon degeneration corrects pretarget topographic sorting errors. Neuron 78:49-56.

Scholes JH (1979) Nerve fibre topography in the retinal projection to the tectum. Nature 278:620-624.

Shigeoka T, Jung H, Jung J, Turner-Bridger B, Ohk J, Lin JQ, Amieux PS, Holt CE (2016) Dynamic Axonal Translation in Developing and Mature Visual Circuits. Cell 166:181-192.

Shirvan A, Kimron M, Holdengreber V, Ziv I, Ben-Shaul Y, Melamed S, Melamed E, Barzilai A, Solomon AS (2002) Anti-semaphorin 3A antibodies rescue retinal ganglion cells from cell death following optic nerve axotomy. J Biol Chem 277:49799-49807.

Simpson HD, Kita EM, Scott EK, Goodhill GJ (2013) A quantitative analysis of branching, growth cone turning, and directed growth in zebrafish retinotectal axon guidance. J Comp Neurol 521:1409-1429.

Sperry RW (1963) Chemoaffinity in the Orderly Growth of Nerve Fiber Patterns and Connections. Proc Natl Acad Sci U S A 50:703-710.

Stuermer CA (1988) Retinotopic organization of the developing retinotectal projection in the zebrafish embryo. The Journal of neuroscience : the official journal of the Society for Neuroscience 8:4513-4530.

Suster ML, Kikuta H, Urasaki A, Asakawa K, Kawakami K (2009) Transgenesis in zebrafish with the tol2 transposon system. Methods Mol Biol 561:41-63.

Thelen K, Maier B, Faber M, Albrecht C, Fischer P, Pollerberg GE (2012) Translation of the cell adhesion molecule ALCAM in axonal growth cones - regulation and functional importance. J Cell Sci 125:1003-1014.

Tryon RC, Pisat N, Johnson SL, Dougherty JD (2013) Development of translating ribosome affinity purification for zebrafish. Genesis 51:187-192.

Welshhans K, Bassell GJ (2011) Netrin-1-induced local beta-actin synthesis and growth cone guidance requires zipcode binding protein 1. The Journal of neuroscience : the official journal of the Society for Neuroscience 31:9800-9813.
Yao J, Sasaki Y, Wen Z, Bassell GJ, Zheng JQ (2006) An essential role for beta-actin mRNA localization and translation in Ca2+-dependent growth cone guidance. Nature neuroscience 9:1265-1273.
Yasuda M, Tanaka Y, Ryu M, Tsuda S, Nakazawa T (2014) RNA sequence reveals mouse retinal transcriptome changes early after axonal injury. PLoS One 9:e93258.
Yasuda M, Tanaka Y, Omodaka K, Nishiguchi KM, Nakamura O, Tsuda S, Nakazawa T (2016) Transcriptome profiling of the rat retina after optic nerve transection. Sci Rep 6:28736.
Ymlahi-Ouazzani Q, O JB, Paillard E, Ballagny C, Chesneau A, Jadaud A, Mazabraud A, Pollet N (2010) Reduced levels of survival motor neuron protein leads to aberrant motoneuron growth in a Xenopus model of muscular atrophy. Neurogenetics 11:27-40.
Zhou J, Wen Y, She L, Sui YN, Liu L, Richards LJ, Poo MM (2013) Axon position within the corpus callosum determines contralateral cortical projection. Proc Natl Acad Sci U S A 110:E2714-2723.
Zivraj KH, Tung YC, Piper M, Gumy L, Fawcett JW, Yeo GS, Holt CE (2010) Subcellular profiling reveals distinct and developmentally regulated repertoire of growth cone mRNAs. J Neurosci 30:15464-15478.
Zolessi FR, Poggi L, Wilkinson CJ, Chien CB, Harris WA (2006) Polarization and orientation of retinal ganglion cells in vivo. Neural Dev 1:2.

Figure legends

Figure 1: Knockdown of Hermes causes topographic guidance defects of RGC dorsal axons.

Zebrafish embryos were fixed at 5 dpf and the eyes injected dorsally (D) with DiI (red) and ventrally (V) with DiO (green) to visualize the retinotectal projections (A). Whole-mount embryos injected with CoMO or HeMO were visualized in lateral (B1-B2; C1-C2) or dorsal view (B3, C3). Hermes depleted embryos show misprojections of dorsal axons in the medial tract (C1, C2, white arrows), that are not present in embryos injected with CoMO (B1, B2). Quantifications show a significant increase of the percentage of embryos showing misprojections in the optic tract (OT) (D). HeMO injected embryos show aberrant projection of dorsal axons entering the tectum through the ventral branch (C3), compared to CoMO (B3). Quantifications show that significantly more dorsal axons misroute and enter the tectum through the ventral branch in Hermes-depleted embryos compared to control (E). HeMO injected embryos were co-injected with a construct expressing full length myc-tagged *Xenopus* Hermes (He-myc) (F). After 72hpf, immunostainings show a strong myc signal in the RGC layer (RGCL). Co-injection of

He-myc rescues the dorsal axons misprojections in the optic tract observed in HeMO injected embryos (G), with a significant reduction of the percentage of embryos with defects (H). In HeMO injected embryos, some dorsal axons enter in the tectum through the medial tectum (J1-J2) and this mistargeting is absent in He-myc co-injected embryos (K1-K2). Quantifications show a rescue of misprojecting dorsal axons in He-myc injected embryos (L). Error bars represent SEM. Numbers of embryos analyzed are indicated on bars. Scale bars 50 µm.

Figure 2: Hermes exerts a negative translational control of specific mRNAs in RGCs.
Increase in puromycin incorporation detected by Western blotting in Hermes depleted condition compared to control (A, B). The GFP expression is restricted to the eye in the atoh7:rpl10a-GFP transgenic line (C1, C1'), with a positive signal in Zn-5 positive RGCs and photoreceptors (C2, C3). 72hpf atoh7:rpl10a-GFP embryos, injected with CoMO or HeMO, were homogenized and immunoprecipitations against GFP were performed on lysates. The total RNA was then extracted from the ribosome-mRNA complexes, analyzed by bioanalyzer, and quantified by qPCR (D). Quantifications show an increase of *nadl1.1, nadl1.2, alcama, alcamb, nrp1a* and *nrp1b* mRNAs bound to ribosomes in absence of Hermes (E). Quantifications of total RNAs input show no difference between CoMO and HeMO conditions (F). *nrp1 in situ* hybridization on 72hpf retinal transverse sections show no difference between CoMO and HeMO injected embryos (G). Quantifications of signal intensity show no difference in *nrp1* expression in HeMO compared to CoMO (G). mRNAs levels were calculated by using the formula $2^{\wedge}$-ΔΔCt with *beta-actin* mRNA as a calibrator (E, F). Error bars represent SEM. Number of embryos analyzed are indicated on bars. Scale bars 30 µm (C2, C3), 100 µm (G).

Figure 3: Hermes depletion increases Nrp1 protein in axons and induces an earlier response to Sema3A.
Immunostainings on stage 32 *Xenopus* retinal explants show increased Nrp1 expression on Hermes depleted growth cone compared to control (A). Quantifications show a significant increase in Nrp1 signal intensity in the growth cone at stage 28 (B), stage 32 (C), stage 35/36 (D) and stage 39 (E). Eye explants were cultured from stage 32 and 35/36 *Xenopus* embryos for 24 hours. Sema3A was added for 10min before fixation and the percentage of collapsed growth cones were counted (F). BSA (Bovine serum albumin) was used as a control. Examples of collapse response of control and Hermes-depleted growth cones (G). At stage 32, Hermes-depleted growth cones display a significantly higher collapse response to Sema3A compared to

control (H). This increase in collapse response is not present at stage 35/36 (I). Error bars represent SEM. Numbers of growth cones analyzed are indicated on bars. Scale bars 100 µm.

Figure 4: Restoring Nrp1 levels rescues the dorsal axon topography defect in Hermes-depleted embryos.

Nrp1 immunostaining on retina transverse sections from atoh7:gapRFP zebrafish embryos injected with CoMO (A), HeMO (B) or HeMO+Nrp1MO (C). Quantifications show a significant increase of Nrp1 signal intensity in HeMO condition compared to CoMO and HeMO+Nrp1MO (D). Lateral view of whole-mount DiI and DiO injected retina from CoMO (E), HeMO (F) and HeMO+Nrp1MO (G) injected embryos. HeMO+Nrp1MO co-injected condition show a significant reduction of the percentage of embryos with mistargeting in the optic tract compared to HeMO (L). Error bars represent SEM. Numbers of embryos analyzed are indicated on bars. Scale bars 100 µm (A-C). Scale bars 50 µm (E-G; I-K).

FIGURE 1

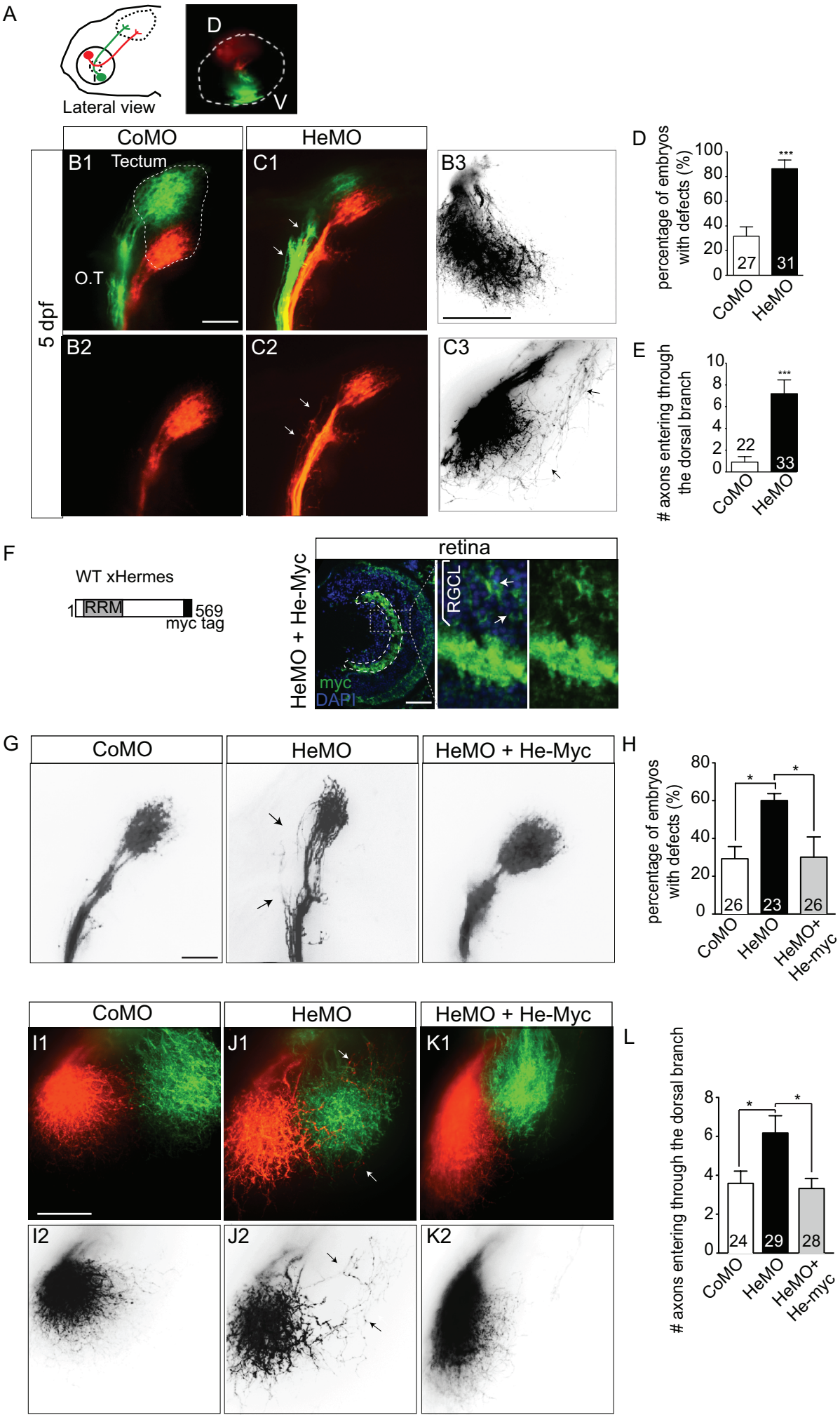
A
Lateral view
D
V
CoMO
HeMO
B1
Tectum
O.T
C1
B3
5 dpf
B2
C2
C3
D
percentage of embryos with defects (%)
100
80
60
40
20
0
27
31
***
CoMO
HeMO
E
axons entering through the dorsal branch
10
8
6
4
2
0
22
33
***
CoMO
HeMO
F
WT xHermes
1
RRM
569
myc tag
retina
HeMO + He-Myc
RGCL
myc
DAPI
G
CoMO
HeMO
HeMO + He-Myc
H
percentage of embryos with defects (%)
80
60
40
20
0
*
*
26
23
26
CoMO
HeMO
HeMO+ He-myc
I1
J1
K1
I2
J2
K2
L
axons entering through the dorsal branch
8
6
4
2
0
*
*
24
29
28
CoMO
HeMO
HeMO+ He-myc

FIGURE 2

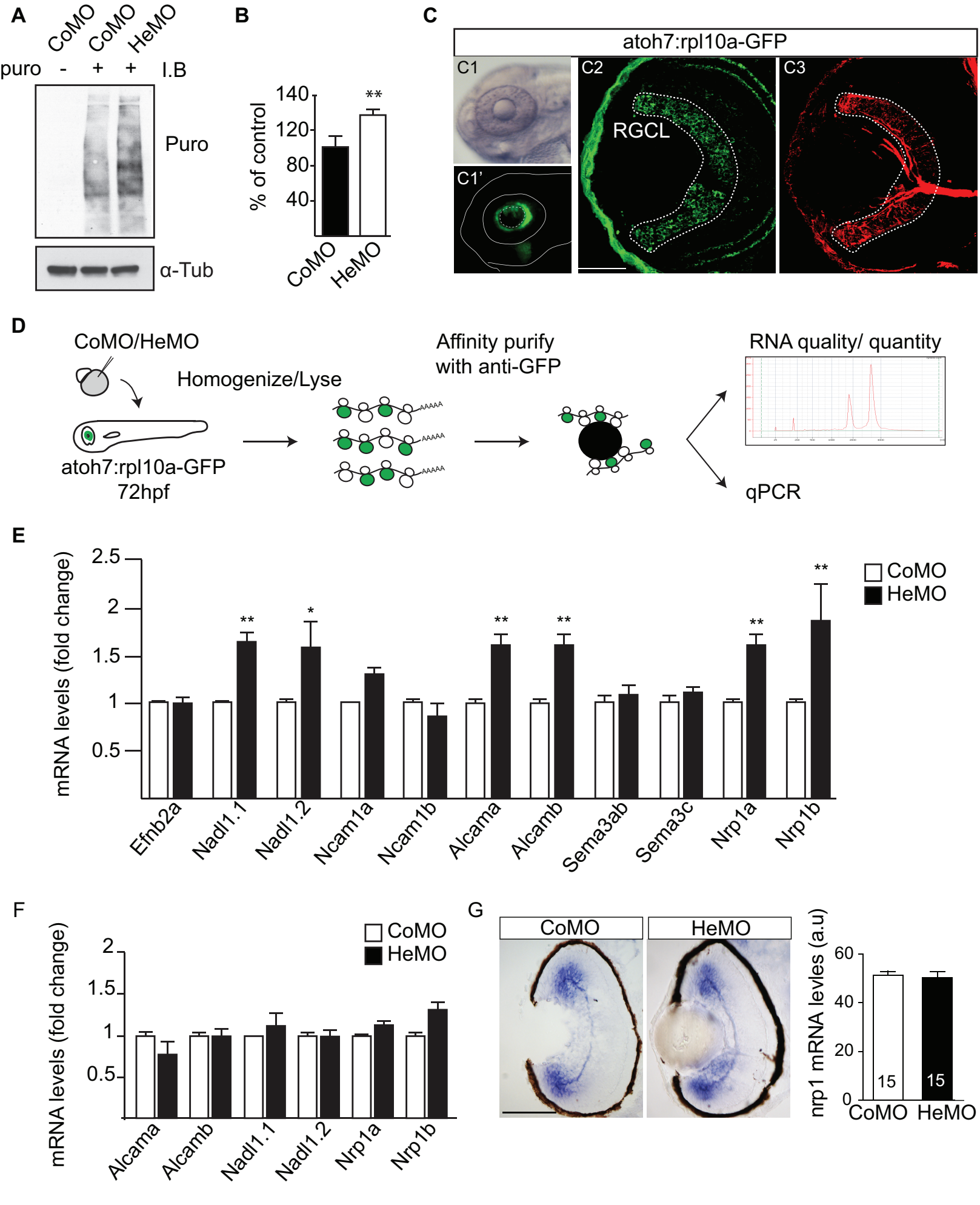
A
CoMO
CoMO
HeMO
puro - + + I.B
Puro
α-Tub
B
% of control
140
120
80
40
**
CoMO
HeMO
C
atoh7:rpl10a-GFP
C1
C1'
C2
RGCL
C3
D
CoMO/HeMO
Homogenize/Lyse
atoh7:rpl10a-GFP
72hpf
Affinity purify
with anti-GFP
RNA quality/ quantity
qPCR
E
mRNA levels (fold change)
2.5
2
1.5
1
0.5
CoMO
HeMO
Efnb2a
Nadl1.1
Nadl1.2
Ncam1a
Ncam1b
Alcama
Alcamb
Sema3ab
Sema3c
Nrp1a
Nrp1b
F
mRNA levels (fold change)
2
1.5
1
0.5
CoMO
HeMO
Alcama
Alcamb
Nadl1.1
Nadl1.2
Nrp1a
Nrp1b
G
CoMO
HeMO
nrp1 mRNA levles (a.u)
60
40
20
0
15
15
CoMO
HeMO

FIGURE 3

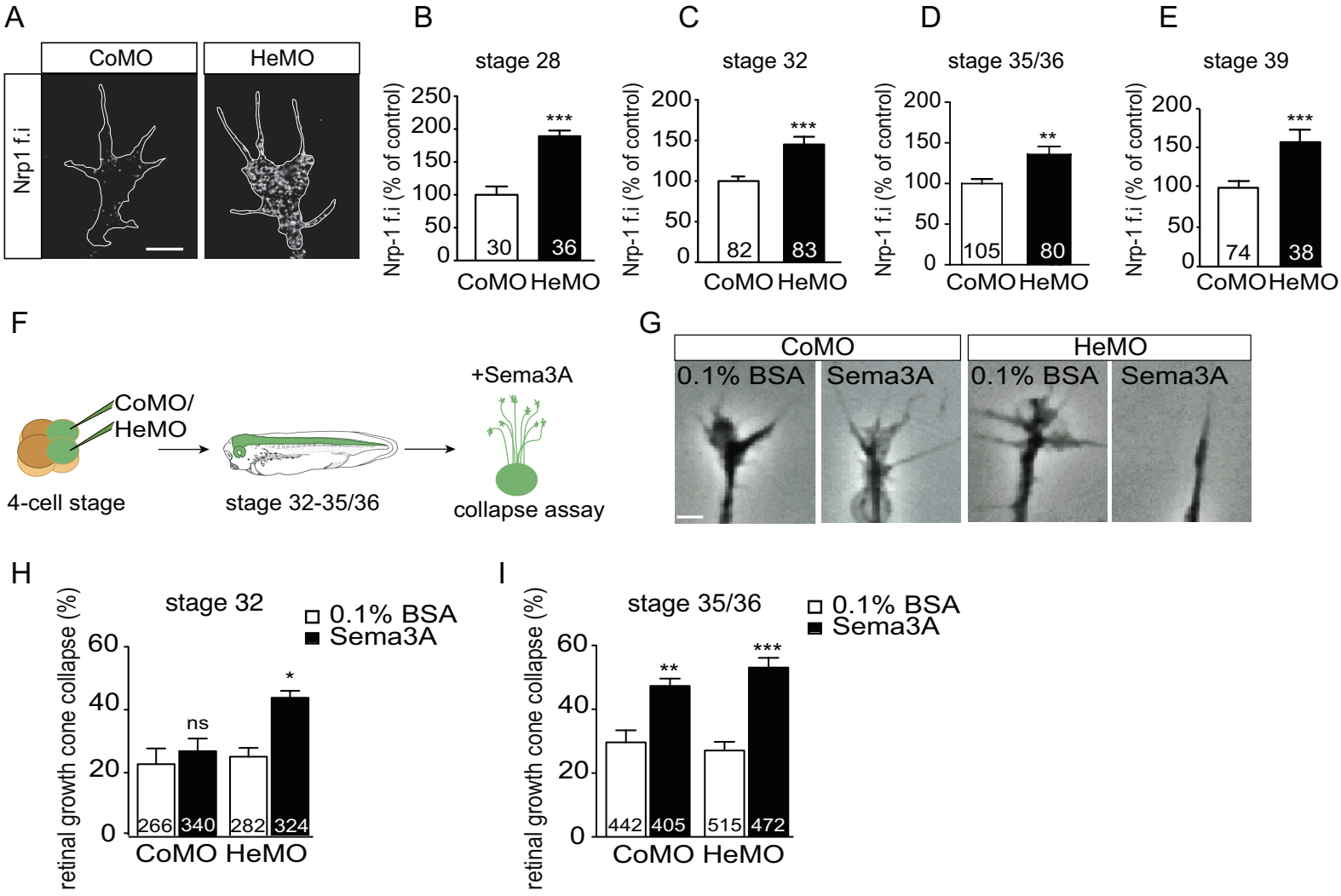
A
CoMO
HeMO
Nrp1 f.i
B
stage 28
Nrp-1 f.i (% of control)
250
200
150
100
50
0
***
30
36
CoMO HeMO
C
stage 32
Nrp-1 f.i (% of control)
200
150
100
50
0
***
82
83
CoMO HeMO
D
stage 35/36
Nrp-1 f.i (% of control)
200
150
100
50
0
**
105
80
CoMO HeMO
E
stage 39
Nrp-1 f.i (% of control)
200
150
100
50
0
***
74
38
CoMO HeMO
F
CoMO/
HeMO
4-cell stage
stage 32-35/36
+Sema3A
collapse assay
G
CoMO
HeMO
0.1% BSA
Sema3A
0.1% BSA
Sema3A
H
stage 32
0.1% BSA
Sema3A
retinal growth cone collapse (%)
60
40
20
0
ns
*
266
340
282
324
CoMO HeMO
I
stage 35/36
0.1% BSA
Sema3A
retinal growth cone collapse (%)
60
40
20
0
**
***
442
405
515
472
CoMO HeMO

FIGURE 4

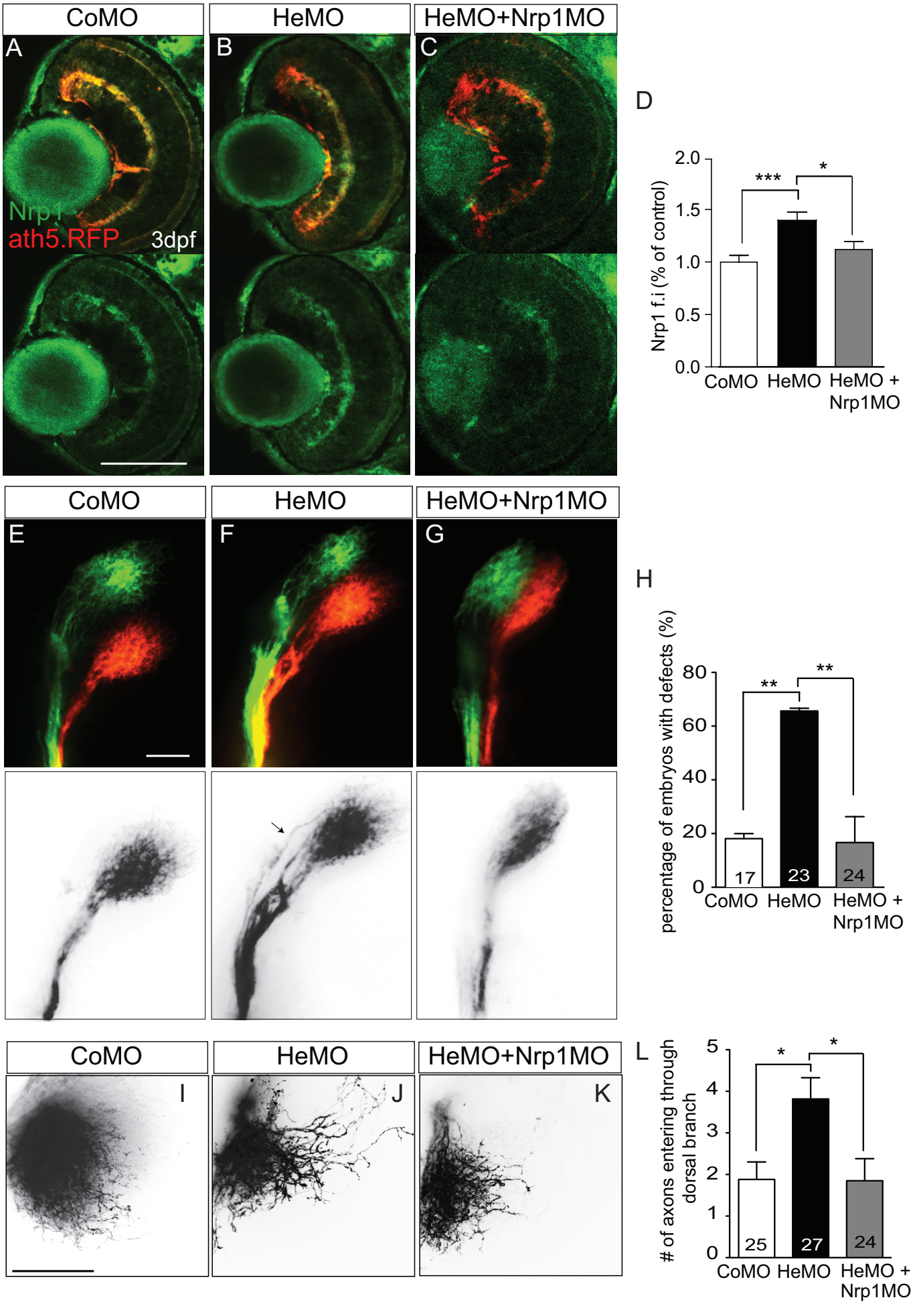
CoMO
HeMO
HeMO+Nrp1MO
A
B
C
Nrp1
ath5.RFP
3dpf
D
Nrp1 f.i (% of control)
2.0
1.5
1.0
0.5
0.0
***
*
CoMO
HeMO
HeMO + Nrp1MO
E
F
G
H
percentage of embryos with defects (%)
80
60
40
20
0
**
**
17
23
24
I
J
K
L
# of axons entering through dorsal branch
5
4
3
2
1
0
*
*
25
27
24